

Plasma Sci. Technol. **25** (2023) 125102 (8pp) https://doi.org/10.1088/2058-6272/ace87d

The advance of magnetic diagnostics system in support of EAST long-pulsed operation

Dalong CHEN (陈大龙)[1,*], **Biao SHEN** (沈飙)[1,*], **Tonghui SHI** (石同辉)[1], **Bihao GUO** (郭笔豪)[2], **Tingyu LI** (李婷玉)[1], **Lixing CHEN** (陈力行)[1], **Minmin XUE** (薛敏敏)[3] **and Nan CHU** (楚南)[1]

[1] Institute of Plasma Physics, Chinese Academy of Sciences, Hefei 230031, People's Republic of China
[2] College of Physics and Optoelectronic Engineering, Shenzhen University, Shenzhen 518060, People's Republic of China
[3] School of Optoelectronic Engineering, Guilin University of Electronic Technology, Guilin 541004, People's Republic of China

E-mail: cdalong@ipp.ac.cn and biaoshen@ipp.ac.cn

Received 5 June 2023, revised 17 July 2023
Accepted for publication 18 July 2023
Published 15 September 2023

Abstract

In EAST long-pulsed discharge (hundreds of seconds), electric magnetic diagnosis (EMD) is very important, since EMD not only monitors tokamak security status but also provides accurate measurement accuracy for reconstruction of the plasma boundary. To avoid current measurement drift, a fiber optic current sensor, based on the Faraday effect, is developed and used for poloidal and plasma current feedback control for the first time, relative current measurement accuracy is within 0.5%. To ensure plasma boundary control accuracy, a detailed set of magnetic measurement calibration methods is developed before the plasma discharge. The maximum relative error is less than 1%, the corresponding control accuracy is within 1 cm. To minimize integrator drift error, a long-pulse integrator test is essential, the corresponding drift error needs to be subtracted in plasma control system. Besides, the saddle coil and Mirnov coil not only help to detect MHD issues, but are also utilized for plasma disruption prediction during the long-pulse discharge.

Keywords: EAST, magnetic diagnostics, MHD, disruption, FOCS

(Some figures may appear in colour only in the online journal)

1. Introduction

In magnetically confined plasma, magnetic measurement is mainly used for the detailed reconstruction of plasma equilibrium, since it could provide plasma position, loop voltage, plasma shape and plasma current [1, 2]. These parameters are critical for plasma control, since we do not want the plasma to touch the wall and disrupt. Magnetic measurement is a simple and mature diagnostic tool, and has been introduced in other tokamaks over the years [3–5]. However, some details including magnetic probe installation, calibration of magnetic measurements, and upgrade of plasma current measurement are still worthy of describing. Some experience accumulated from the long-pulse discharges still holds guiding significance for ITER and future devices.

EAST is a superconducting tokamak, that has a flexible plasma configuration, such as limiter plasma and divertor plasma, including lower single null (LSN), upper single null (USN), and double null (DN) [6, 7]. In the plasma ramp-up phase, R_P, Z_P, I_P (RZIP) control is applied in a limited plasma configuration. Later, the plasma shape transits into ISOFLUX control at 0.4 s, at which point the magnetic measurement becomes significantly important in the overall plasma control. In the last two years, both 1000 s super I-mode discharge and

* Authors to whom any correspondence should be addressed.

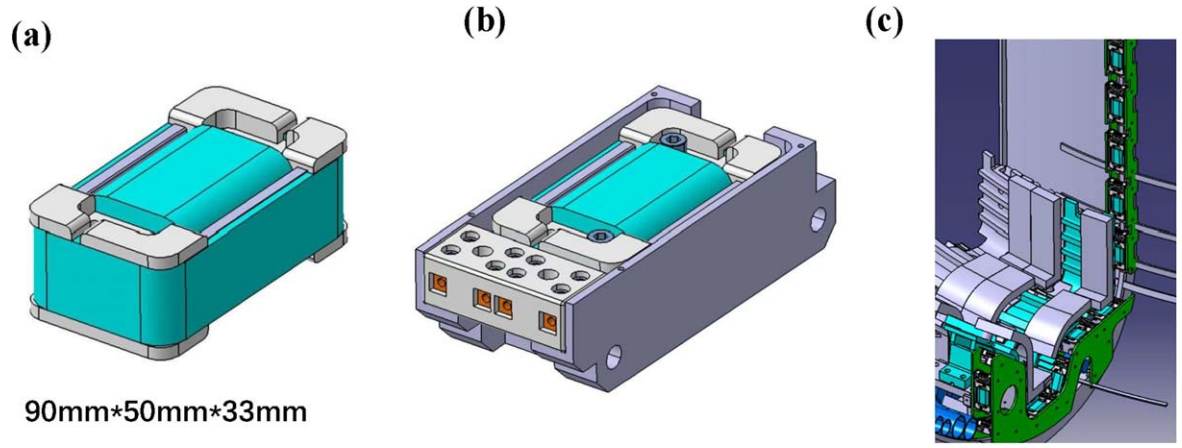

Figure 1. Subplot (a) is the design of a 2D magnetic probe; subplot (b) is the assembly of the probe and the stainless steel protective cover; and subplot (c) is the installation of probes on the vacuum vessel.

400 s H-mode discharge have been achieved in EAST. This requires a higher precision magnetic measurement. To ensure that the magnetic probe provides reliable and accurate experimental data, the magnetic diagnostic system, including probe production, installation and calibration method, has been greatly improved. The relative measurement error is within 1% (less than the control error of 3%), and the corresponding control accuracy is within 1 cm.

To minimize the measurement error of the current, a closed-loop fiber optic current sensor (FOCS) has been successfully used in tokamak plasma current measurements and current feedback control [8, 9]. Until now, poloidal field current, in-vessel fast coil current and plasma current are all measured by using FOCS and for feedback control. For poloidal field current measurement, considering the adjacent busbar can contribute large magnetic crosstalk to the sensor, the interfering Faraday phase shift is inversely proportional to the distance (from the fiber optic closure point to the interfering current conductor). The experiment shows that a measurement accuracy of 0.4% can be achieved when the gap is larger than 200 mm. For plasma current measurement, considering the severe working conditions the FOCS withstands, the installation of FOCS and the protection process of optical fibers have been both improved, which ensures the fibers will not be damaged by arcing. Finally, the relative measurement error is within 0.5%.

This paper is structured as follows: section 2 describes the design, installation and calibration of magnetic probes; section 3 describes the upgrade of FOCS; and section 4 describes the MHD detection and disruption prediction model using the loop voltage, saddle coil signal and Mirnov coil signal.

2. Magnetic probe design and calibration

2.1. Probe design and assembly

A magnetic probe is a reliable method to measure the magnetic field surrounding the plasma and to detect MHD issues. In order to better utilize the inner vacuum vessel space, normally the probe is made into a two-dimensional structure, as shown in figure 1. The probe skeleton is made of ceramic ($95\#Al_2O_3$), since the ceramic has the advantage of high hardness, wear resistance, and good erosion resistance. The winding cable is made of polyimide material with a diameter of 1 mm. The winding cable is rated a maximum service temperature of 380 °C, which is higher than the vacuum baking temperature of 200 °C. The cable is wound on the ceramic tightly in an even number of coils for reducing the magnetic crosstalk. Before the probe is installed around the vacuum vessel it first needs to be fixed with a stainless cover, because ceramics are more fragile than stainless steel. After the probe is matched with the shielding box, it will be installed in the groove support as a whole and fixed with pins. Recent five campaigns have shown that this installation method can effectively ensure the poloidal consistency of the probe (perpendicular to the toroidal field), and the position of the calibrated probe will not be changed anymore, this can effectively ensure accurate reconstruction of the plasma configuration. Figure 2 shows the EAST probe installation process and post-installation probe distribution diagram. Considering that the divertor structure (tungsten/copper structure) not only has a certain electromagnetic shielding effect, but also the magnetic field at the X-point is relatively weak. Therefore, during the installation process, the probe is installed adjacent to the divertor structure, between the two cassettes, and is consistent with its plasma configuration. In the long-pulse experiments, the operator could move the X-point smoothly and avoid an excessive arise in local heat load.

For the magnetic probe, especially for the Mirnov coil, knowing the frequency curve of the probe is crucial for MHD physical analysis. The magnetic coil is placed in the Helmholtz coil, in the whole test circuit, there is a high-frequency generator. By measuring the induced voltage of the probe and the voltage of the Hertzholm coil, the amplitude–frequency curve of the probe can be obtained, and then the resonant frequency of the probe can be obtained. Furthermore, there is a long-distance signal transmission between the probes and

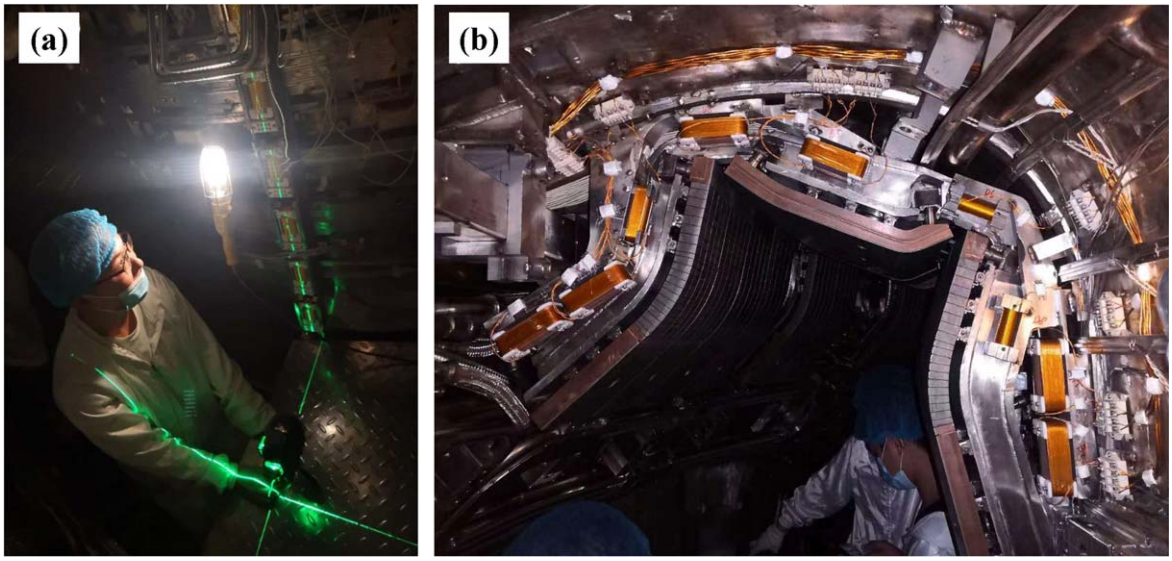

Figure 2. (a) Probe installation process and (b) distribution of magnetic probe at the divertor area.

the signal acquisition units (~70 m), a series of resonant frequencies of the magnetic probe and the one connected to the transmission line should be both tested separately. Figure 3 shows that the resonant frequencies of the individual probe are 325 kHz and 410 kHz, respectively, when the twisted pair is not connected. After the twisted pair is connected, the resonant frequency is significantly reduced to 60 kHz and 70 kHz, since twisted pair cables could contribute a large inductive impedance in the circuit. Nonetheless, even with the additional transmission cables, the working frequency of the probe still meets the control requirements at present (10 kHz). However, for high-frequency magnetic probes, the acquisition unit must be placed directly near the device, and a coaxial cable is used for signal transmission instead.

2.2. Calibration of magnetic probe

The calibration of the magnetic probe is critically needed before every plasma campaign [10]. On one hand, calculations can be used to verify the positive and negative signs of measured values. On the other hand, experiments with a vacuum shot can help calibrate errors in the entire electromagnetic measurement system, which may come from position calibration deviation or the signal processing unit. Normally, some vacuum shots with pure poloidal field currents and multiple sets of poloidal field currents were conducted. Figure 4 shows the benchmark of the calculated value $B_{\text{cal.}}$ with the measurement $B_{\text{mea.}}$:

$$B_{\text{cal.}} = G \times I_{\text{PF}} \tag{1}$$

where G is the matrix of the Green function between the poloidal field current and magnetic probe, I_{PF} is the poloidal field current. The magnetic field measurement can be expressed as:

$$B_{\text{mea.}} = \frac{V}{NS} \times \frac{RC}{G} \tag{2}$$

where V is the output voltage of the probe, NS is the effective induced area of the probe, in EAST $NS \sim 0.2$ m^2, RC is 20 ms, and G is magnification. Taking an example of the No. 1 probe, as shown in figure 4, the Y-axis represents the error between the measured and the calculated values. X-axis is the calculated value. The linear error is within 0.1%, and the random uncertainties are less than 20 Gs. Normally the random uncertainties come from the effective area of the probe and integration time constant. Considering that EAST is aiming at long-pulse discharge, the integration time constant should not be too small, and experiments have shown that $RC = 20$ ms is acceptable for long-pulse discharge. The relative error between the measured and calculated values can be expressed:

$$B_{\text{mea.}} - B_{\text{cal.}} = k \times B_{\text{cal.}} + b. \tag{3}$$

In the actual calibration experiment, b is close to 0. Then, the $B_{\text{cal.}} = \frac{1}{k+1} \times B_{\text{mea.}}$. In the calibration experiment, we need to calibrate the linear slope of each probe and make corrections in the plasma control system (PCS). In fact, the systematic bias of k is caused by signal transmission, the signal integrator, etc. In each calculation, the value of k is very small, so only a few probe coefficients need to be corrected.

For plasma current measurement, the Rogowski coil is an effective method [11, 12]. The basic approach for estimating plasma current is Ampere's law. It can be simply rewritten as:

$$I_{\text{p}} = \frac{1}{\mu_0} \oint B_{\text{p}} \cdot \text{d}l \tag{4}$$

where I_{p} is the plasma current, B_{p} is the poloidal magnetic field. The integrated route should be a closed contour that encircles the plasma region. For ITER, due to the long length of the Rogowski coil around the inner vacuum vessel, an excessively long coil increases the probability of damage. Therefore, as an alternative, a plasma current can be evaluated by integrating a discrete poloidal probe [13]. In EAST, due to the restriction of installation space, the poloidal probes are not installed tightly together. In order to construct a closed

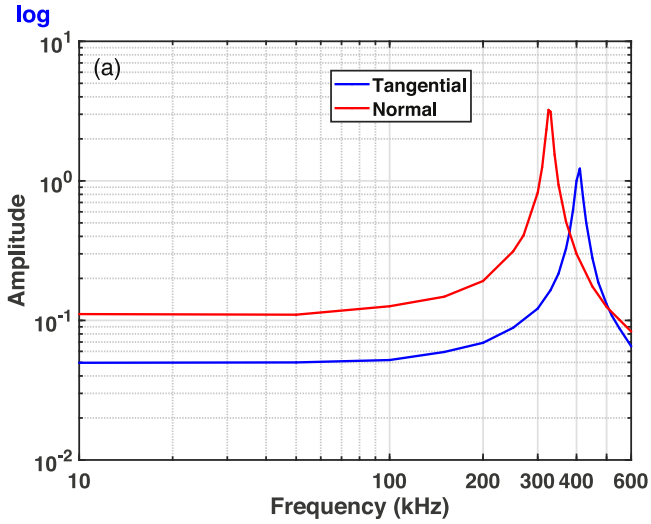

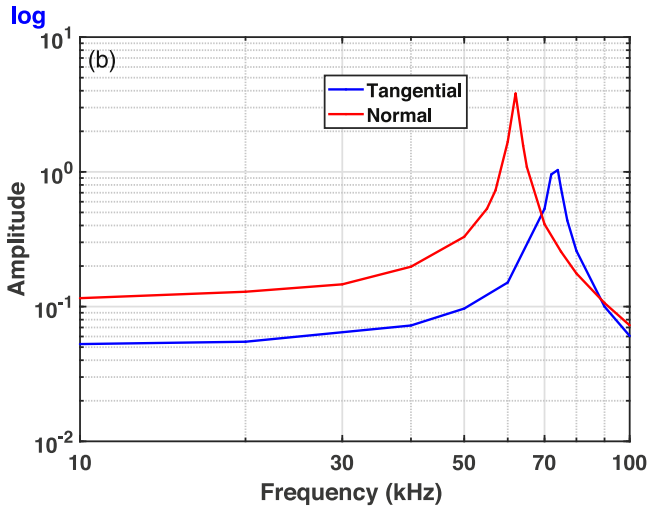

Figure 3. Amplitude–frequency curve of the probe (a) without and (b) with long-distance signal transmission.

integration path, we find the intersection by extending the direction of the magnetic field. Figure 5(a) is a simple schematic diagram of the magnetic integration path, so the plasma current can be calculated by:

$$I_{\mathrm{p-cal}} = \frac{1}{\mu_0}\sum_{1}^{N} B_{\mathrm{p}n} \cdot l_n \tag{5}$$

where $B_{\mathrm{p}n}$ is the poloidal magnetic field of No. n, l_n is the distance between the intersection of extension lines adjacent to the probe. Figure 5(b) is a poloidal complete integration path. Note that, some probes, such as Nos. 17 and 29, were abandoned and did not participate in the calculation due to their installation positions deviating from the integration path. Figure 6 shows a comparison between the plasma current measured by the Rogowski coil and the one calculated by the poloidal magnetic probe. The relative error is within 2%. These results demonstrated here also support the measurement accuracy of the probes.

In the long-pulse discharge, integrator drift testing is essential [14]. The test experiment found that the drift amplitude of the integrator is affected by the current

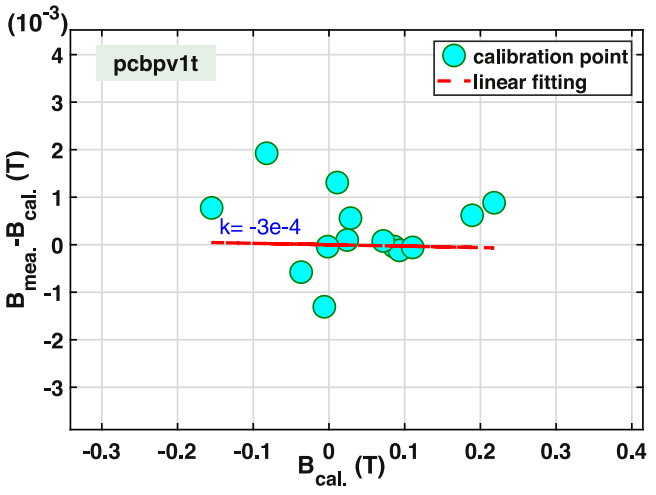

Figure 4. Measured dispersion versus calculated value.

experimental conditions. The temperature drift of the probe varies even at different times of the day. Therefore, it is essential to conduct integrator drift testing prior to initiating long pulses. By compensating for the slope, the drift of the 1000 s integrator is reduced from 100 mV to within 10 mV when the integrator time constant is 20 ms.

3. Fiber-optic current sensor

Based on the Faraday effect and not dependent on the integrator, the fiber-optic current sensor can achieve long-term current measurement and is a promising current method [15, 16]. Different types of coating for optical fibers were tested in Tore Supra [17] and JET [18], the FOCS measurements present a very good linearity with respect to the plasma current and long-term stability. The basic principle can be written as:

$$\theta = VN\oint_L \vec{B}(l)\cdot \mathrm{d}\vec{l} = \mu VNI \tag{6}$$

where θ is the rotation of angle, V is the Verdet constant for the optical fiber, N is the number of loop turns surrounding the conductor and I is the measured current. The total Faraday rotation angle is obtained by integrating the local Faraday rotation along the optical fiber. The local Faraday rotation depends on the local Verdet constant, which in turn depends on the local temperature. In EAST plasma operation, the sensing fiber was installed behind the first wall, the working temperature for the spun fiber varies ranging from 30 °C to 45 °C since the divertor structure was equipped with a water-cooling system. The Verdet constant depends on the local temperature and has a temperature drift, however, the measurement error can be compensated by adjusting the retarder retardation, and the combined contribution is ignored when the change in working temperature is small. Considering that the manufacturing of the sensor head still depends on the local temperature, all the optical fiber systems will be tested in an environment ranging from −50 °C to 100 °C before leaving the factory. It is found that the relative error is less

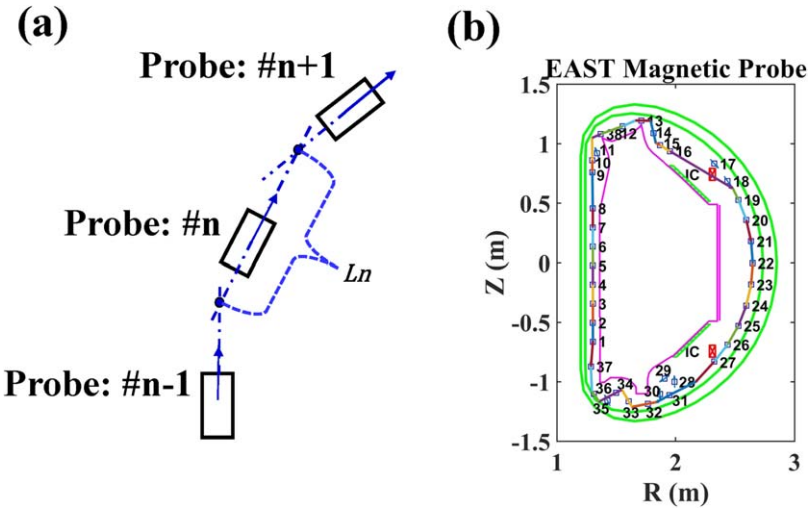

Figure 5. (a) Schematic diagram of magnetic field integration and (b) EAST magnetic probe poloidal integration path.

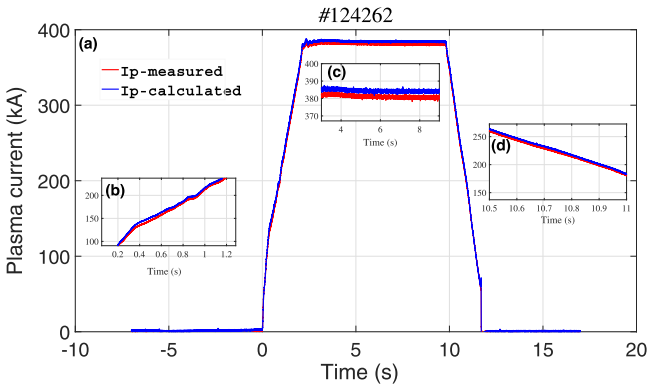

Figure 6. Comparison results of plasma current between the measurement by using Rogowski coil and the calculation by using a poloidal magnetic probe. (a) Overall comparison, (b) local comparison in the start-up period, (c) local comparison in the flat-top period and (d) local comparison in the ramp-down period.

than 0.2%, which meets the measurement requirements. A detailed description of the relationship between the Verdet coefficient and temperature is introduced in [9]. A series of tests of the fiber at higher temperatures (200 °C–300 °C) will be carried out next. So far, after several thousand discharges, the FOCS measurements are in very good agreement with the Rogowski coil data in EAST.

Figure 7 is a typical set-up of a reflective FOCS. The light emitted by the light source becomes linearly polarized light after passing through the polarizer, and the linearly polarized light is uniformly divided into two beams of orthogonal linearly polarized light after passing through a 45-degree angle welding point. After being modulated by a phase modulator, the two beams of orthogonal linearly polarized light are, respectively, converted into left-handed circularly polarized light and right-handed circularly polarized light through a quarter-wave retarder. The two beams of forward circularly polarized lights enter the sensing optical fiber, and a Faraday phase difference is generated under the action of a magnetic field generated by a current to be measured. Since there is a reflector at the end of the sensing fiber, the Faraday phase difference in the two beams of circular polarization light is doubled.

In EAST, a reflective FOCS with a phase shift closed-loop control system was developed by SWT OPTICS Co., Ltd. The sensor was first installed on the inner vacuum vessel in 2016. With regard to the reflective FOCS, since circularly-polarized light is transmitted twice in the sensing fiber coil, this doubles the output signal, yields higher sensitivity to FOCS, and achieves a smaller nonlinear error during high current measurement. In the whole FOCS system for fusion devices, two points are very critical for the measurement. One is the characteristics of the sensing fiber. Since the fiber will survive in the vacuum vessel for a long time, the suitable working temperature for sensing fiber (SLB 1250) is below 85 °C, and can survive up to 300 °C for a short time. Therefore, the protection of fiber and working temperature control should be improved in the future, possibly the water-cooled structures for fiber optics can be considered in future plans. Another consideration is the feed-through of the fiber. Since fiber is very sensitive and weak, unable to withstand high squeezing. In the EAST experiment, a component epoxy was designed for fiber and was used for flange pouring, which can ensure a good sealing performance. However, in the future fusion device, the working temperature of epoxy will increase to a hundred degrees, so a new sealed method should be considered.

In the 2021 EAST campaign, a reflective FOCS was first used for plasma current feedback and played a decisive role in the thousand-second plasma experiment. As shown in figure 8, during the 1065 s discharge, the plasma current decreased from 340 kA to 200 kA, which is not accepted for the plasma control system. In comparison, the FOCS shows good accuracy and long-term stability. Unfortunately, in the subsequent long-pulse operation with higher RF injection (H-mode, $P_{RF} \sim 4.5$ MW), both sets of optical fibers located in the lower field side were seriously damaged, this may be caused by energetic particle or arc effect. The melted PEEK protective sleeve can be seen in the subgraph of figure 9. Additionally, there are some signs of erosion on the surface of the stainless hose.

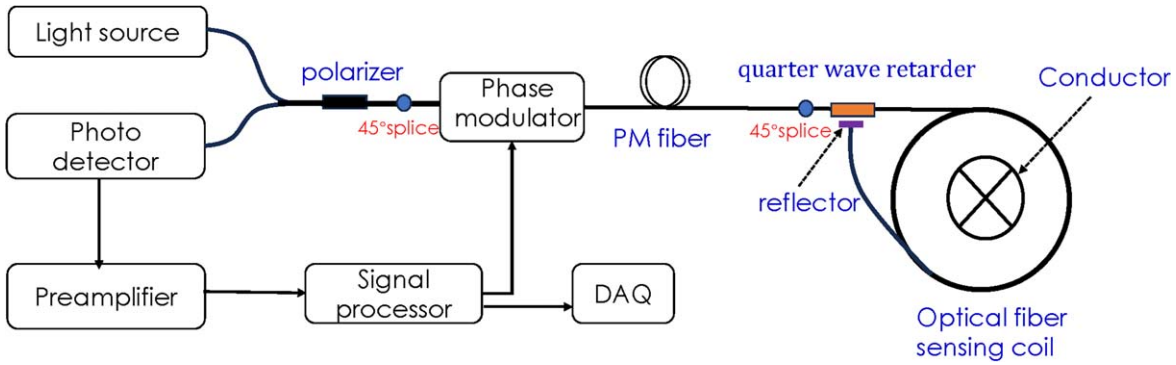

Figure 7. Typical set-up of reflective FOCS.

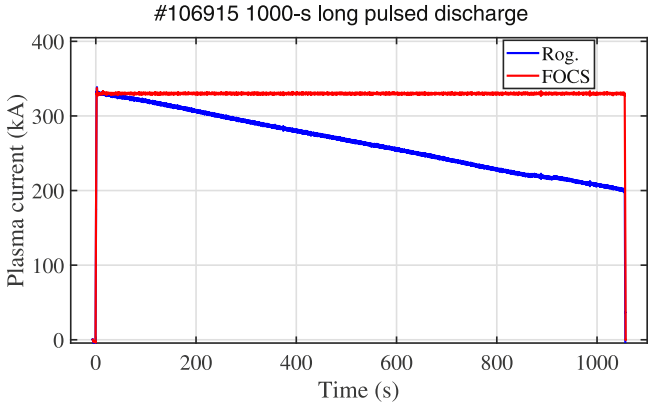

Figure 8. Comparison of plasma current measured by Rogowski coil and the one measured by FOCS in the 1065 s discharge.

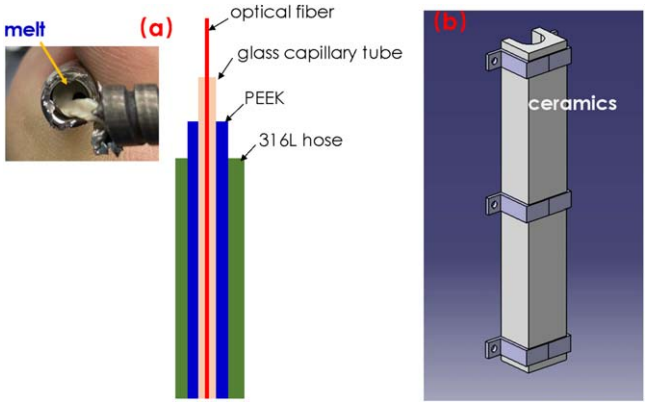

Figure 9. Damaged sensing fiber (subplot). (a) The upgraded protection for fiber and (b) the newly designed protection cover.

In the subsequent upgrade, a glass capillary tube (~850 μm) was added to protect the sensing fiber. Considering the glass capillary tube is very fragile, the PEEK tube was still retained and sheathed outside the glass tube. Additionally, a section of ceramic shielding was used to protect the optical fiber in the lower field side, the details of which can be seen in figure 9. In the 2023 experiment, repetitive 400 s H-mode discharges were achieved by using the new upgraded FOCS. Up until now, the system has demonstrated a perfect measurement performance, having experienced thousands of discharges.

4. MHD detection and disruption prediction using magnetic sensors

4.1. Low frequency detect

In addition to being used for plasma control, electromagnetic measurement can be applied for MHD detection and plasma disruption prediction. Figure 10 illustrates a typical discharge experiencing a low-frequency MHD event (the low-frequency Mirnov coils were installed in the midplane position on the low-field side between every two ports) and which ultimately leads to plasma disruption. In this discharge, the plasma current is 600 kA, $q_{95} = 4.2$. Starting from 4.69 s, an $m/n = 2/1$ tearing mode with a frequency of 3 kHz was triggered, which quickly grew to a large scale, simultaneously the mode frequency decreased and finally dropped to zero, as depicted in figure 10 (right). During the tearing mode period, the core temperature slightly decreased. When the tearing mode was locked, $n = 1$ radial magnetic field, extracted from the saddle coil, began to increase quickly. The lock mode survived for 50 ms. In the process of the lock mode, the core plasma temperature was decreasing continuously, even though sometimes the temperature was reheated by the RF wave. Until 4.79 s, when $\frac{B_r}{B_t} \sim 8 \times 10^{-5}$, a thermal quench occurred, causing a significant amount of thermal energy to be lost to the first wall. The plasma was ultimately disrupted due to the decrease in temperature and the increase in plasma resistance.

4.2. High-frequency detect

In addition to low-frequency Mirnov probes, additional high-frequency Mirnov probes with a sampling rate of 1 MHz are available at adjacent K and L ports. These can be used for the detection of high-frequency MHD modes, such as: Alfvén Eigenmodes (AEs) [19–21], Geodesic Acoustic Modes (GAM) [22], fishbone modes, kink modes, etc. Figure 11 shows the first observation of the Toroidal Alfvén Eigenmode (TAE) from 120 kHz to 180 kHz in a spectrogram detected from high-frequency sampling Mirnov probes [23]. The TAE mode is driven by energetic electrons in EAST's low-density ohmic discharges when resonant magnetic perturbation (RMP) forces magnetic reconnection/penetration. The TAE mode may disappear under higher plasma density because a higher collisional rate will dampen the energetic electrons that drive it.

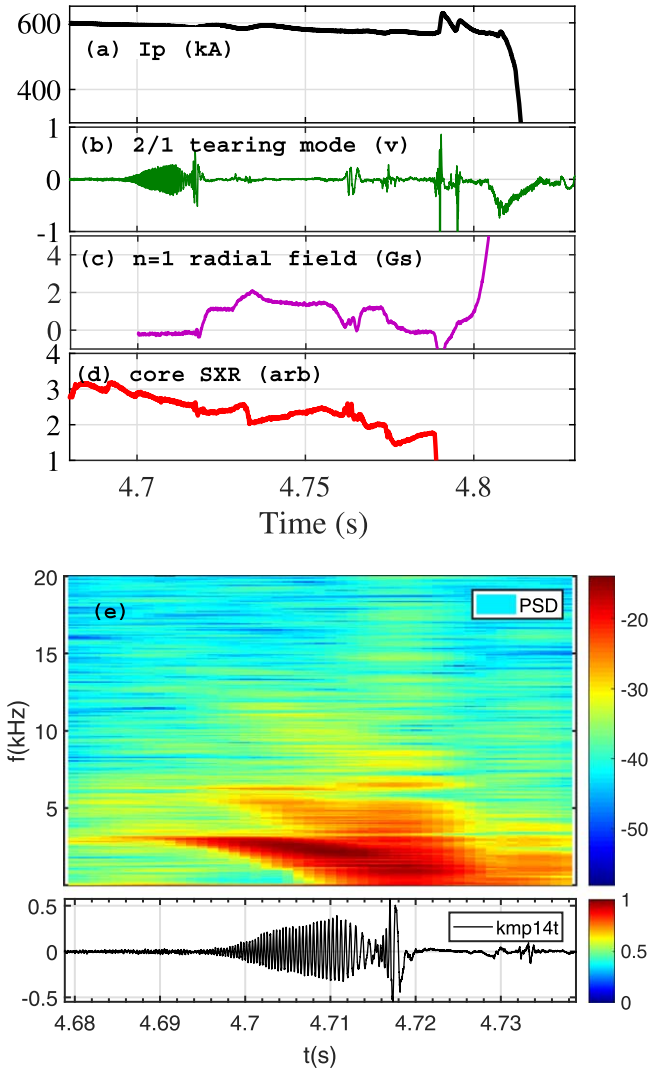

Figure 10. An example of a disruption case caused by MHD issues (left). (a) Plasma current, (b) tearing mode detected by Mirnov coil, (c) radial magnetic field extracted from saddle coil, (d) core soft-x ray and (e) spectrogram of Mirnov signal.

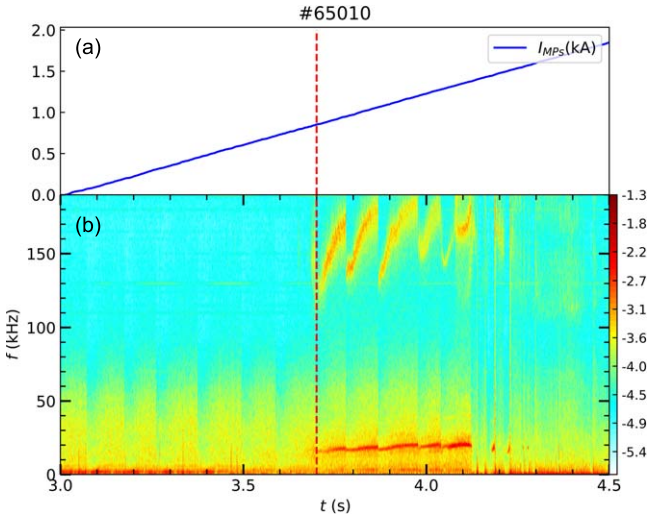

Figure 11. Toroidal Alfvén Eigenmode (from 120 kHz to 180 kHz) induced by RMP. (a) Waveform of RMP and (b) spectrogram detected from high frequency sampling Mirnov probes.

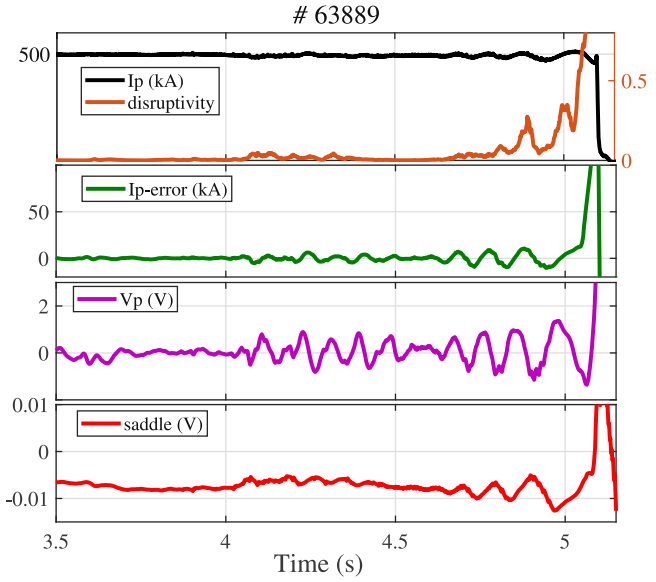

Figure 12. An example of a disruption shot, showing the evolution between the possibility of disruption and corresponding change of magnetic signals (I_p error, loop voltage, saddle signal).

4.3. Disruption prediction model

For the disruption prediction model, to detect early MHD events before a disruption, many magnetic signals are selected to be added into the prediction model [24, 25], such as plasma current, saddle coil array, Mirnov coil array, loop voltage, and so on. The disruption prediction database demonstrates that a significant number of loop voltage values and I_p error values (the error between measured plasma current and programmed plasma current) increase rapidly during the ∼100 ms before a disruption occurs. Figure 12 shows a typical disruption discharge. Starting from 4 s, the possibility of disruption is closely related to magnetic diagnostics, particularly I_p error, loop voltage and saddle signal. Starting at 4.5 s, the possibility of disruption is highly sensitive to these three signals. In the disruption prediction model, certain relevant magnetic measurements can be used for disruption analysis and real time warnings.

5. Conclusions

With the update to the first wall structure [26] and the increase in RF heating power [7], the EAST magnetic diagnostics system has been significantly improved. The accumulated experience during the upgrade process remains essential for ITER and future devices [27]. To improve measurement accuracy, it is essential to subtract the linear part of the system error of the magnetic probe based on the data of vacuum shot without plasma. The major improvements are as follows: (1) During long-term baking and discharges, it was found that the wire made of glass and mica can easily carbonize and gradually harden, resulting in decreased insulation. In the past five EAST campaigns with high-power auxiliary heating, the polyimide

cable has been used as probe winding instead, offering good insulation performance in high-temperature and radiation environments. In addition, the probe fixing support with groove style is very effective for probe positioning and fixation. The error in the upgraded electromagnetic measurement has consistently remained within 1%. (2) For the probe near the divertor, it is advantageous to install the probe along the divertor structure, a necessity for accurate control of the plasma X-point. (3) Reflective optical fibers possess a higher modulation speed and measurement bandwidth, along with reduced nonlinear errors. Therefore, the FOCS demonstrates stable performance in plasma current measurement and plays an important role in long-pulse plasma control. Note that, during the installation process, the fiber optic protection on the low-field side should not be ignored, ceramics provide excellent radiation and erosion-resistant protective shells. Additionally, it should be noted that the local Faraday rotation depends on the local Verdet constant, which in turn depends on the local temperature. Consequently, the impact of wide-ranging temperature changes on fiber optic current sensors needs to be considered and tested as promptly as possible. (4) During long pulses, certain magnetic measurement signals can be utilized for low-frequency and high-frequency mode detection, and they can also be incorporated into the disruption warning model for safer operation control.

Acknowledgments

This work is supported by the National Magnetic Confinement Fusion Program of China (Nos. 2018YFE0302100 and 2022YFE03010002) and National Natural Science Foundation of China (Nos. 12205195).

References

[1] Lao L L *et al* 1985 *Nucl. Fusion* **25** 1611
[2] Lao L L *et al* 2005 *Fusion Sci. Technol.* **48** 968
[3] Strait E J 2006 *Rev. Sci. Instrum.* **77** 023502
[4] Lee S G *et al* 2008 *Rev. Sci. Instrum.* **79** 10F117
[5] Moreau P *et al* 2018 *Rev. Sci. Instrum.* **89** 10J109
[6] Xiao B J *et al* 2012 *Fusion Eng. Des.* **87** 1887
[7] Xu G S *et al* 2021 *Nucl. Fusion* **61** 126070
[8] Xue M M *et al* 2019 *Fusion Eng. Des.* **140** 11
[9] Xue M M *et al* 2019 *Fusion Eng. Des.* **148** 111264
[10] Liu G J *et al* 2013 *Rev. Sci. Instrum.* **84** 073502
[11] Moreau P *et al* 2015 *Fusion Eng. Des.* **96–97** 878
[12] Chen D L *et al* 2015 *Rev. Sci. Instrum.* **86** 103506
[13] Bak J G *et al* 2022 *Fusion Eng. Des.* **185** 113324
[14] Wang Y *et al* 2014 *Fusion Eng. Des.* **89** 618
[15] Gusarov A *et al* 2018 *Fusion Eng. Des.* **136** 477
[16] Gusarov A *et al* 2023 *Fusion Eng. Des.* **192** 113626
[17] Moreau P *et al* 2011 *Fusion Eng. Des.* **86** 1222
[18] Leysen W *et al* 2020 *Fusion Eng. Des.* **160** 111754
[19] Zhang T *et al* 2018 *Plasma Sci. Technol.* **20** 115101
[20] Xu M *et al* 2020 *Nucl. Fusion* **60** 112005
[21] Zhao J Q *et al* 2021 *Plasma Sci. Technol.* **23** 095101
[22] Xu M *et al* 2021 *Nucl. Fusion* **61** 106008
[23] Chu N *et al* 2018 *Nucl. Fusion* **58** 104004
[24] Guo B H *et al* 2021 *Plasma Phys. Control. Fusion* **63** 025008
[25] Guo B H *et al* 2021 *Plasma Phys. Control. Fusion* **63** 115007
[26] Luo G N *et al* 2017 *Nucl. Fusion* **57** 065001
[27] Wan Y X *et al* 2017 *Nucl. Fusion* **57** 102009